Available online at www.sciencedirect.com

SCIENCE DIRECT

Thin Solid Films 479 (2005) 232–237

www.elsevier.com/locate/tsf

Optical and microstructural properties of nanocomposite Au/SiO_2 films containing particles deformed by heavy ion irradiation

J.-M. Lamarre[a], Z. Yu[b], C. Harkati[b], S. Roorda[b], L. Martinu[a,*]

[a]*Department of Engineering Physics, École Polytechnique de Montréal, CP 6079, succ. Centre-Ville, Montréal, Québec, Canada H3C 3A7*
[b]*Physics Department, Université de Montréal, CP 6128, succ. Centre-Ville, Montréal, Québec, Canada H3C 3J7*

Received 4 June 2004; accepted in revised form 22 November 2004
Available online 7 January 2005

Abstract

Gold nanoparticles embedded in a dielectric matrix (SiO_2) were prepared by a hybrid technique combining plasma-enhanced chemical vapor deposition and pulsed DC sputtering. The concentration and spatial distribution of the metal particles were controlled by deposition parameters, while particle size and size distribution were further adjusted by annealing. Subsequently, the nanocomposite samples were exposed to an energetic ion beam (30 MeV), a treatment that has been shown to transform spherical particles to high aspect ratio ellipsoids. The films were studied in detail by spectroscopic ellipsometry and spectrophotometry, and their optical response was correlated with their microstructural features such as particle alignment in the ion beam direction, as documented by the blue shift of the surface plasmon resonance (SPR). We show that such process is reversible in a sense that subsequent annealing of ion beam-irradiated particles red shifts the SPR to the initial position.

Pacs: 78.20.-e; 78.66.Sq
Keywords: Nanostructures; Gold; Ion bombardment; Surface plasmons

1. Introduction

New developments in optical technology and telecommunications require novel materials for both active and passive photonics devices; this includes waveguides, interferometers, and switches. Nanocomposite (NC) films consisting of metal particles such as gold [1–5,9,10,12–15], silver [5,6,11], and copper [5,7,8,11] embedded in a dielectric matrix have recently been the subject of many studies motivated by observed large third-order nonlinearity as reported by Ricard et al. [16]. This follows complementary investigations [1,2,17,18] in which NC metal–dielectric systems have been considered for their interesting color effects in decorative applications, their adjustable electrical conductivity, and their magnetic properties (for a review, see [18]). Surface plasmon resonance (SPR) of gold nanoparticles is also of great interest in biomedical sensor applications [19]. NC films can be prepared with various metal concentrations and particle sizes using different fabrication techniques; this includes sputtering [3,4,8–10,12], sol–gel [6], colloidal solutions [5], ion implantation [7], hybrid methods combining, for example, plasma-enhanced chemical vapor deposition (PECVD) and sputtering [2,13–15], and other methods [11].

One of the main limitations encountered in the preparation of NC metal–dielectric systems is the lack of control of the size and shape of the metal particles in the matrix. Particle size evolution upon postdeposition annealing has been extensively studied by Dalacu and Martinu [13–15] using spectroscopic ellipsometry (SE). The authors demonstrated that SE is a technique of choice for the characterization of such nanostructured films since it allows one to precisely determine the microstructural features by means of a nondestructive optical measurement.

In the present paper, we propose a new method that allows one to further control the shape of the particles of an

* Corresponding author. Tel.: +1 514 340 4099; fax: +1 514 340 3218.
E-mail address: lmartinu@polymtl.ca (L. Martinu).

0040-6090/$ - see front matter © 2004 Elsevier B.V. All rights reserved.
doi:10.1016/j.tsf.2004.11.180

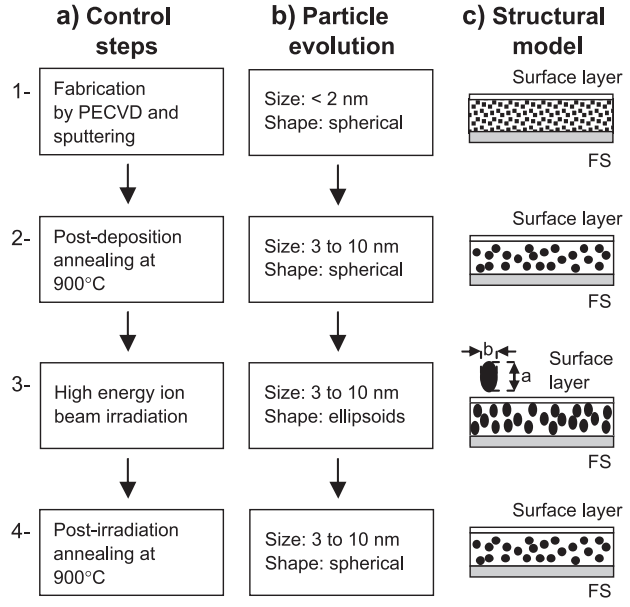

Fig. 1. Illustration of the film preparation steps, evolution of the particle size and shape, and corresponding microstructural models.

NC system. As a proof of principle, gold and SiO_2 are described in this work, but other combinations have also been successfully tested. We show that using a heavy ion beam irradiation of the NC sample, one is able to change the particle shape from spheroids to prolate spheroids. This control of microstructure allows one to select with high precision the position of the SPR band either by a size-related red shift or a shape-related blue shift.

2. Sample preparation and characterization

2.1. Film fabrication

The films were prepared by a hybrid process simultaneously combining PECVD and pulsed DC sputtering. The substrates (c-Si and fused silica) were placed on an RF-powered (13.56 MHz) substrate holder electrode on which negative substrate bias voltage V_B develops. The working gas flow consisted of 30 sccm Ar, 20 sccm O_2, and 5 sccm SiH_4, while the total pressure was maintained at 8 Pa (60 mTorr). The RF power applied was 40 W corresponding to V_B=−300 V. Gold was simultaneously sputtered from a 50 mm gold target (99.99% purity) installed on a magnetron head located at a 15 cm distance from the substrate. The gold concentration was controlled by the total power delivered to the target from a pulsed DC power supply (Pinnacle Plus; Advanced Energy) using a pulse frequency of 350 kHz. The deposition conditions were optimized in order to obtain high-quality, low-absorption (extinction coefficient k smaller than 10^{-5} at 550 nm) SiO_2, as well as high mechanical stability and hardness ($H \geq 7$ GPa). Typical thickness of the films was about 500 nm.

In order to further modify the film microstructure, the fabrication process continued with three subsequent steps, as illustrated in Fig. 1. After the initial deposition (step 1), postdeposition annealing (step 2) was used to control the particle size. The samples were annealed in the ambient atmosphere at temperatures ranging from 600 to 900 °C for different times. In step 3, ion bombardment was used to further modify the particle shape. The samples were exposed, at room temperature, to a 30 MeV Cu^{5+} ion beam using a Tandem linear accelerator. The doses ranged from 10^{13} to 10^{15} ions/cm^2, with a beam current of 200 nA. In the case of core–shell colloidal particles, such treatment has been shown to elongate the gold particles along the direction parallel to the ion beam (see Fig. 1c) [20]. Further annealing (step 4) is then performed in order to study the reversibility of the ion irradiation process.

2.2. Optical characterization

Optical properties of the films were determined from spectrophotometry (Lambda-19; Perkin-Elmer) and variable-angle SE (VASE; J.A. Woollam) measurements. In order to derive the optical characteristics of the films, we applied an ellipsometric model consisting of the substrate, the NC layer, and the surface roughness layer (see Fig. 1c).

In our model, gold permittivity ε_m was described by the Drude equation by taking into account the intraband transitions:

$$\varepsilon_m(\omega) = 1 - \frac{\omega_p^2}{\omega(\omega + i\Gamma)}. \quad (1)$$

Here ω_p and Γ are, respectively, the plasma frequency and the effective collision frequency. Γ is defined as:

$$\Gamma = \frac{1}{\tau_B} + \frac{Av_F}{R} \quad (2)$$

where τ_B, A, v_F, and R represent the free electron relaxation constant, the broadening parameter, the Fermi velocity, and the particle radius. The interband region of the spectra was modeled using Lorentz oscillators:

$$\varepsilon_m(\omega) = \varepsilon_\infty + \sum_k \frac{A_k}{E_k^2 - (\hbar\omega)^2 - iB_k\hbar\omega}. \quad (3)$$

For the k^{th} oscillator, A_k is the amplitude, E_k is the oscillator energy position, and B_k indicates the broadening of the oscillator.

Real $n(\lambda)$ and imaginary $k(\lambda)$ parts of the complex refractive index of the silica matrix were fitted using a three-parameter Cauchy dispersion curve:

$$n(\lambda) = A + \frac{B}{\lambda^2} + \frac{C}{\lambda^4}, \quad (4)$$

while the absorption was taken into account by a three-parameter Urbach absorption tail:

$$k(\lambda) = \alpha e^{\left(\beta\left(\frac{1}{\lambda}-\frac{1}{\gamma}\right)\right)}. \quad (5)$$

In Eqs. (4) and (5), A, B, and C are fit parameters, and α, β, and γ are, respectively, the extinction coefficient amplitude, the exponent factor, and the band edge. Fused silica substrates were also fitted using the Cauchy dispersion model. One should note that the absorption due to both the matrix and the substrate is much lower than the absorption related to gold.

Effective medium approximation (EMA) is well suited for modeling our films since the particle size is much lower than the probe wavelength [17]. For low gold concentrations (several volume percent), such as in this study, we can apply the well known Maxwell–Garnett model [21,22]:

$$\frac{\varepsilon_{\text{eff}} - \varepsilon_{\text{h}}}{\varepsilon_{\text{eff}} + 2\varepsilon_{\text{h}}} = p\frac{\varepsilon_{\text{m}} - \varepsilon_{\text{h}}}{\varepsilon_{\text{m}} + 2\varepsilon_{\text{h}}}, \quad (6)$$

where ε_{eff} is the effective permittivity, while ε_{m} and ε_{h} are the permittivities of the metal and the matrix, respectively. p is the gold filling factor (vol.%). Surface roughness was modeled by the use of an EMA layer consisting of 50% void/50% NC layer. In such way, we could derive from the combined spectrophotometry and SE measurements the film thickness, gold concentration, particle size, optical properties (n and k), and roughness.

The deformed particles with a nonspherical shape were accounted for in the ellipsometric model by using a depolarization factor for prolate spheroids ($a>b=c$; see Fig. 1c):

$$L_z = \frac{1-e^2}{e^2}\left[\frac{1}{2e}\ln\left(\frac{1+e}{1+e}\right) - 1\right], \quad (7)$$

with

$$e^2 = 1 - b^2/a^2. \quad (8)$$

Here, $L_x=L_y$ and $L_x+L_y+L_z=1$, while z is normal to the film surface. The depolarization factor was incorporated in the Maxwell–Garnett model by calculating the polarizability of an ellipsoid and its local electric field [23,24]:

$$\frac{\varepsilon_{\text{eff}}^{j} - \varepsilon_{\text{h}}}{L_j\varepsilon_{\text{eff}}^{j} + (1-L_j)\varepsilon_{\text{h}}} = p\frac{\varepsilon_{\text{m}} - \varepsilon_{\text{h}}}{L_j\varepsilon_{\text{m}} + (1-L_j)\varepsilon_{\text{h}}}. \quad (9)$$

The index j in Eq. (9) stands for the three directions x, y, and z.

2.3. Complementary microstructural characterization

In addition to optical measurements, the film microstructure was evaluated by transmission electron microscopy (TEM; CM30 Philips microscope) on samples prepared by ion polishing (PIPS), atomic force microscopy (AFM; Digital Instruments), X-ray diffraction (XRD; Philips X'Pert-MPD), and Rutherford backscattering (RBS; 2 MeV He ions).

3. Results and discussion

Fig. 2 shows an example of ellipsometric results in terms of measured and fitted ellipsometric angles ψ and Δ for a typical annealed film (after step 2) with p=1.8 vol.%. Agreement between the experimental data and the fit is excellent over the whole spectrum for all three angles. The measurement at a 55° incidence angle is noisier since SE measurements are less sensitive when ψ is close to 0° (corresponding to Δ close to 180° for the 55° angle). Typical roughness values are in the range of 10 nm, in good agreement with AFM measurements. Combined SE and RBS (not shown here) data provide information on the gold

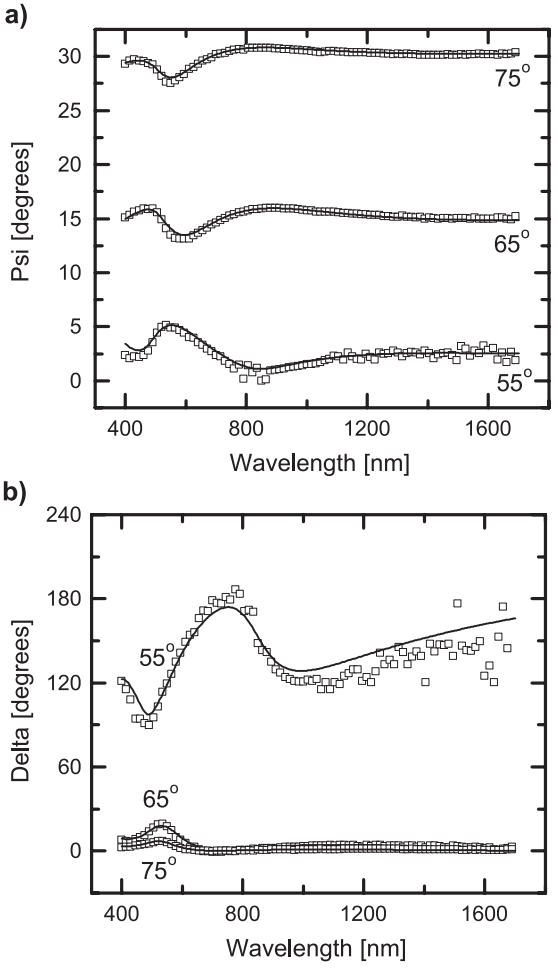

Fig. 2. Examples of spectral dependence of the ellipsometric angles ψ (a) and Δ (b) for three different incidence angles: 55°, 65°, and 75°. Squares indicate experimental data while the full line represents the fit. For better clarity, only one third of the data points is represented. Extracted parameters from the fitted data for this particular sample are the following: thickness 350 nm, surface roughness 17 nm, gold concentration 1.8 vol.%, and particle size 5 nm.

concentration in the films with about 0.2 vol.% precision in the range from 0.5 vol.% up to 20 vol.%.

An example of optical transmission of an as-deposited specimen is shown in Fig. 3a. The SPR cannot be distinguished in the spectra since the gold particle size is lower than 1 nm. Indeed, for very small particles, the collective conduction electron response vanishes as a consequence of the disappearance of the free electron gas. Such small particles could not be seen with TEM even at ×550,000 magnification. However, XRD measurements revealed some evidence of crystalline gold.

In order to obtain particle sizes larger than 2 nm, as required for the development of nonlinear optical properties [3,4,11,12], we annealed the films for 2 h at various temperatures. We found that a minimum anneal temperature (T_A) of 600 °C is needed to activate the diffusion process, which causes the particles to grow. This temperature is comparable to the melting temperature of gold nanoparticles predicted by simulations [25] and confirmed experimentally [14].

As particle size increases (T_A increasing), one can observe a red shift of the SPR (as indicated by the arrow in Fig. 3a).

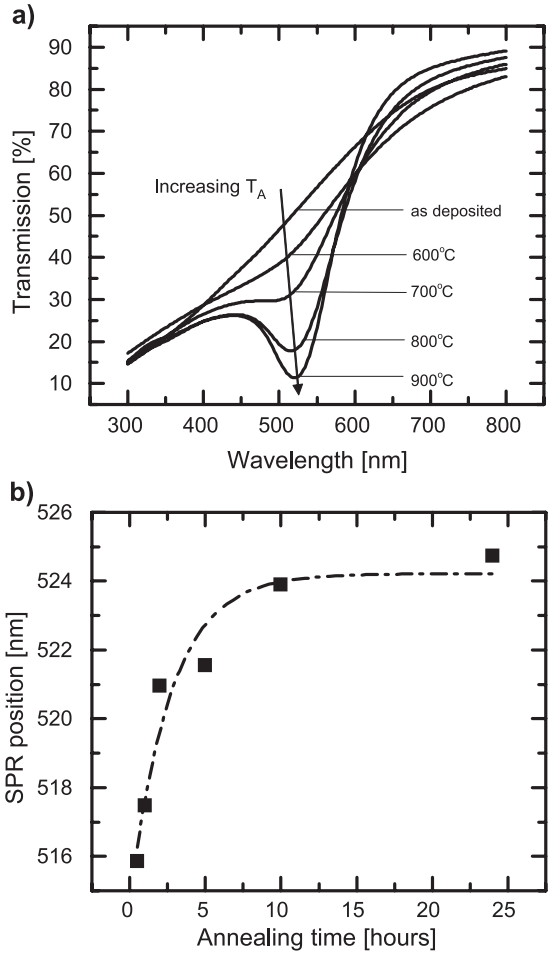

Fig. 3. Evolution of SPR upon annealing. (a) Optical transmission for films annealed for 2 h at different T_A. (b) SPR shift as a function of annealing time at 900 °C.

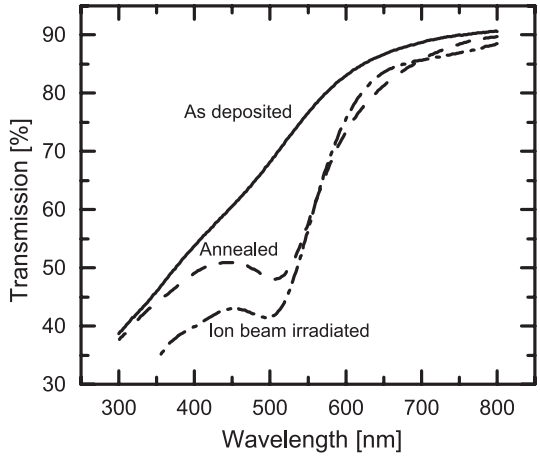

Fig. 4. Transmission spectra for a 1 vol.% gold-containing SiO_2: full line—as-deposited film; dashed line—after 900 °C annealing for 2 h; dashed/dotted line—after 3.5×10^{15} ions/cm^2 ion beam irradiation without annealing.

This red shift is taken into account in the Lorentz oscillators presented in our ellipsometric model. The physics behind the model can be explained in the following way: in the case of small particles of noble metal, d-electron screening red shifts the SPR. Noble metal atoms possess a region of nonoverlap between the d-electron wave function and the conduction electrons. Inside the particle, this nonoverlap is averaged over the unit cell. This statement is not true anymore on the surface of the cluster. As a consequence, if the surface-to-volume ratio decreases, the screening of the d-electrons is enhanced; hence, a red shift is obtained for bigger particles [26,27]. As particle size increases, we also observed a narrowing of the absorption band, which can be attributed to Landau damping and a narrowing of the particle size distribution [28]. In the ellipsometric model, this effect is taken into account by the size dependence of the effective collision frequency in the Drude equation.

We systematically studied the effect of annealing time on the position of the SPR. It can be seen in Fig. 3b that the SPR is red-shifted toward a plateau for increasing annealing times. This can be attributed once again to the growth of the particle size by a diffusion process. It is also interesting to note that after 10 h, the SPR wavelength stops changing, indicating saturation in the particle growth. Fitting the data using an exponential behavior, we obtained a time constant of 2.7 h for this thermally activated process (at T_A=900 °C).

In this work, we studied another way to vary the particle size and shape, namely sample irradiation by an energetic ion beam. Observation of irradiated but not annealed samples (steps 1 and 3) shows that ion beam irradiation causes growth of the particle size as it can be observed from the presence of the SPR in Fig. 4. This result strongly suggests a very high local temperature within the irradiated NC material. Calculations using the SRIM software [29,30] show that the penetration depth of copper ions into the sample (30 MeV) is around 12 μm (0.5 μm thick layer of NC and 11.5 μm in the FS substrate). It is therefore possible

that the local temperature elevation could be restricted to this depth, an effect of particular interest for the deposition on thermally sensitive substrates. This method can also be used in conjunction with other materials combinations (e.g., copper or silver nanoclusters in a silicon nitride matrix), with a lower risk of thermal oxidation of the metal.

Theory predicts a blue shift of the SPR if the particles deform from spheres to ellipsoids aligned in the direction of the propagation of light (in other words, the ellipsoid's smaller axis is parallel to the incident electric field). Using normal incidence irradiation and normal incidence spectrophotometry, we were able to reproduce this shift experimentally. This is illustrated in Fig. 5 featuring the SPR shift as a function of dose for samples with three different p values (p=0.5 vol.%, 1 vol.%, and 2 vol.%). One can readily see that the absorption peak is indeed blue-shifted for higher doses. This suggests that the particle dimension perpendicular to the optical transmission axis becomes smaller. For samples where a longer annealing time was used, the particles became initially larger, and the peak was red-shifted when compared to shorter initial annealing times (compare the 2 and 5 h annealing for p=1 vol.%). One can conclude that the deformation is not a function of the initial particle size.

The deformation effect seems not to be dependent on the gold concentration, at least for low fillings—an effect that is compatible with the deformation mechanism proposed earlier [20]. According to Roorda et al., the ion impact causes strain in the plane perpendicular to the ion beam. Such induced stress then deforms the softer gold particles in the direction parallel to the beam. Our observation in Fig. 5 that the shift saturates as the ion doses increase supports the following explanation: for a constant number of incident ions per unit of time, as the number of ions passed through the layers increases, the strain in the matrix subsequently increases and the forces acting on the gold particles cause them to deform, while relaxing the stresses in the matrix. At

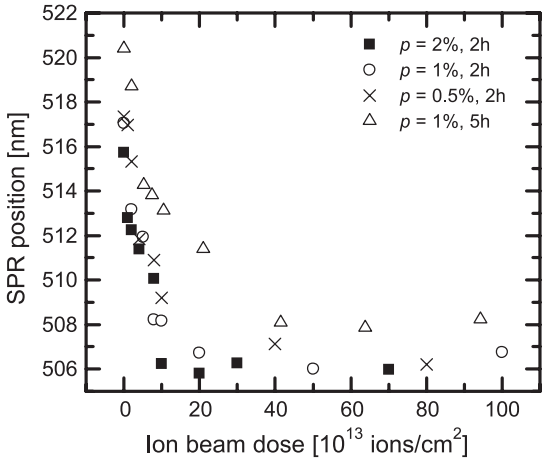

Fig. 5. SPR shift as a function of dose for three different gold concentrations (p=0.5 vol.%, 1 vol.%, and 2 vol.%). The films were annealed at 900 °C for different annealing times prior to ion irradiation as indicated.

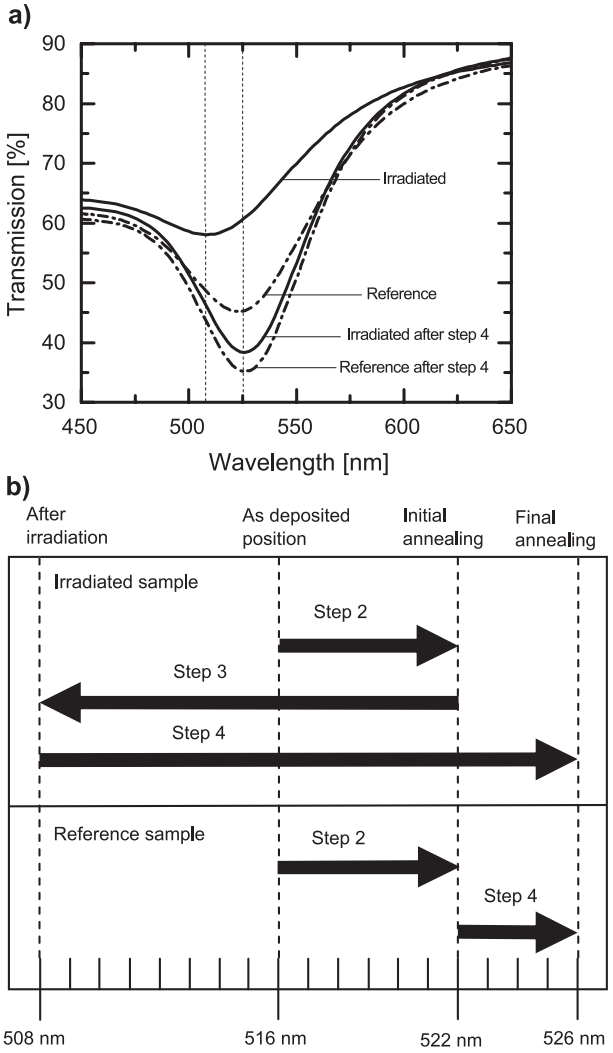

Fig. 6. SPR shift after second annealing. Two identical samples were prepared (steps 1 and 2). The first sample was ion-irradiated (10^{14} ions/cm^2; step 3), while the second one was kept as a reference. Both samples where then annealed at 900 °C (step 4). Final SPR position is the same for both samples. (a) Optical transmission measurements for both samples. (b) Position of the SPR after each step described in Fig. 1.

one point, the deformation of the particles is such that it accommodates the effect of the constant flux of ions, and the matrix is left with enough room in the in-plane direction to relax. Any additional ions have no further deformation effect since a steady state has been reached, at least from the optical point of view. One should point out that the films fabricated in our study contained a much higher gold concentration than those of colloids prepared by Roorda et al. In addition, our films consist of gold particles embedded in a continuous matrix contrary to the Au–silica core–shell particle they studied earlier. Still, the effects observed seem similar.

So far, we have demonstrated that we are able to red shift the SPR with an appropriate annealing, while ion irradiation allows one to blue shift the SPR. In order to further enhance our control on the position of the SPR, we tested postirradiation annealing (step 4). In order to do so, we

have deposited two identical samples (step 1). Both samples were then annealed at 900 °C for 5 h (step 2). One of the samples was implanted (step 3) while the other was kept as a reference. Fig. 6a and b present the SPR position after these different treatments for both samples. After the first annealing, the SPR position is at 522 nm (for both samples). Ion irradiation (step 3) blue shifts the SPR up to 508 nm as a consequence of shape deformation as described previously. One should notice the significant difference of SPR depth between the reference and the irradiated sample in Fig. 6a. This difference is predicted by the generalized Maxwell–Garnett model including the depolarization factor.

Further 2 h annealing at 900 °C was performed on both samples (step 4). This step red shifts the SPR to 526 nm as a consequence of particle growth. Interestingly, the final SPR position is the same for both the ion-irradiated and the nonirradiated sample. We suggest that the final annealing (step 4) changed the shape of the particle from prolate spheroids back to spherical. Small amplitude difference between the spectra of both samples after final annealing (Fig. 6a) can be attributed to a slight difference in thickness.

4. Conclusions

The results of this work can be summarized as follows. We produced high-quality gold/silica nanocomposite films deposited by hybrid PECVD/sputtering deposition. As-deposited samples (step 1) contained particles smaller than 1 nm as determined by TEM, and they exhibited no SPR. High-temperature annealing at 900 °C (step 2) led to a particle size increase above 2 nm, as predicted theoretically. It also gave rise to SPR and to its red shift. Irradiation with high-energy (Cu^{5+}; 30 MeV) ions (step 3) led to two main effects: (1) for unannealed samples, large-enough particles were formed, exhibiting SPR; and (2) for annealed samples, particles were deformed, leading to a blue shift of the SPR. Subsequent annealing (step 4) of samples after ion beam irradiation red-shifted the SPR, most likely because the particles readopted their initial spherical geometry. The combination of annealing and ion beam irradiation thus appears suitable for reproducible adjustment of the SPR position.

Acknowledgements

The authors wish to thank Mr. Gilles Jalbert and Mr. Francis Turcot for their technical support. We would also like to thank Dr. Dan Dalacu for fruitful discussions. This work was supported, in part, by FQRNT (Québec) and NSERC (Canada).

References

[1] J. Perrin, B. Despex, E. Kay, Phys. Rev., B 32 (1985) 719.
[2] L. Martinu, Sol. Energy Mater. 15 (1987) 21.
[3] H.B. Liao, W. Wen, G.K.L. Wong, J. Appl. Phys. 93 (2003) 4485.
[4] S. Debrus, J. Lafait, M. May, N. Pinçon, D. Prot, C. Sella, J. Venturini, J. Appl. Phys. 88 (2000) 4469.
[5] R.A. Ganeev, A.I. Ryasnyansky, Sh.R. Kamalov, M.K. Kodirov, T. Usmanov, J. Phys. D: Appl. Phys. 34 (2001) 1602.
[6] D. Wang, S. Guo, S. Yin, Opt. Eng. 42 (2003) 3585.
[7] M. Falconieri, G. Salvetti, E. Cattaruzza, F. Gonella, G. Mattei, P. Mazzoldi, M. Piovesan, G. Battaglin, R. Polloni, Appl. Phys. Lett. 73 (1998) 288.
[8] G. Battaglin, P. Calvelli, E. Cattaruzza, F. Gonella, R. Polloni, G. Mattei, P. Mazzoldi, Appl. Phys. Lett. 78 (2001) 3953.
[9] H.B. Liao, R.F. Xiao, J.S. Fu, P. Yu, G.K.L. Wong, P. Sheng, Appl. Phys. Lett. 70 (1997) 1.
[10] H.B. Liao, R.F. Xiao, H. Wang, K.S. Wong, G.K.L. Wong, Appl. Phys. Lett. 72 (1998) 1817.
[11] K. Uchida, S. Kaneko, S. Omi, C. Hata, H. Tanji, Y. Asahara, A.J. Ikushima, T. Tokizaki, A. Nakamura, J. Opt. Soc. Am. B 11 (1994) 1236.
[12] I. Tanahashi, Y. Manabe, T. Tohda, S. Sasaki, A. Nakamura, J. Appl. Phys. 79 (1996) 1244.
[13] D. Dalacu, L. Martinu, J. Opt. Soc. Am. B 18 (2001) 85.
[14] D. Dalacu, L. Martinu, Appl. Phys. Lett. 77 (2000) 4283.
[15] D. Dalacu, L. Martinu, J. Appl. Phys. 87 (2000) 228.
[16] D. Ricard, P. Roussignol, C. Flytzanis, Opt. Lett. 10 (1985) 511.
[17] B. Abeles, Appl. Solid State Sci. 6 (1976) 1.
[18] H. Biederman, L. Martinu, in: R. d'Agostino, F. Fracassi, P. Favia (Eds.), Chapter 4 in Plasma Deposition and Treatment of Polymers, Academic Press, San Diego, 1990, p. 269.
[19] D. Yelin, D. Oron, S. Thiberge, E. Moses, Y. Silderberg, Opt. Express 11 (2003) 1385.
[20] S. Roorda, T.V. Dillen, A. Polman, C. Graf, A.V. Blaaderen, B.J. Kooi, Adv. Mater. 16 (2004) 235.
[21] J.C. Maxwell Garnett, Philos. Trans. R. Soc. Lond., A 203 (1904) 385.
[22] J.C. Maxwell Garnett, Philos. Trans. R. Soc. Lond., A 205 (1906) 237.
[23] H.C. Van de Hulst, Light Scattering by Small Particles, Dover Publication, New York, 1981.
[24] R.W. Cohen, G.D. Cody, M.D. Coutts, B. Abeles, Phys. Rev., B 8 (1973) 3689.
[25] L.J. Lewis, P. Jensen, J.L. Barrat, Phys. Rev., B 56 (1997) 2248.
[26] A. Liebsch, Phys. Rev., B 48 (1993) 11317.
[27] V. Kresin, Phys. Rev., B 51 (1995) 1844.
[28] C. Yannouleas, R.A. Broglia, Ann. Phys. (NY) 217 (1992) 105.
[29] J.P. Biersack, L. Haggmark, Nucl. Instrum. Methods 174 (1980) 257.
[30] J.F. Ziegler, The Stopping and Range of Ions in Matter, vols. 2–6, Pergamon Press, 1977–1985.